Int. J. Electrochem. Sci., 10 **(2015)** 10462 - 10477

International Journal of
ELECTROCHEMICAL
SCIENCE
www.electrochemsci.org

Experimental and Modeling Investigation of Pure and Mixed Surfactant Aggregation and Associated Steel Corrosion Inhibition in Aqueous Media

Zhiqiang Ning[1], *Yakun Zhu*[2*], *Michael L. Free*[2]

[1]School of Materials & Metallurgy, Northeastern University, Shenyang 110819, China
[2]Metallurgical Engineering, University of Utah, 135 S 1460 E, Rm 412, Salt Lake City UT, 84112, USA
[*]E-mail: yakun.zhu@utah.edu; ykzhu1@hotmail.com

Received: 14 September 2015 / *Accepted:* 28 September 2015 / *Published:* 4 November 2015

The corrosion issues have led to great interest in industry and academia to control corrosion of metallic pipelines in various oilfields around the world. Among the existing corrosion control methods, surfactant inhibitors have widely been used for corrosion inhibition of metallic pipelines. One model for the prediction of corrosion inhibition efficiency of various pure surfactant and mixed surfactants in aqueous media is developed and validated. The prediction model is based on Langmuir adsorption (LA) sub-model in combination with a critical micelle concentration (cmc) prediction sub-model to create an integrated corrosion inhibition prediction model. The model derivation is introduced by using an example of mixed homologous benzalkonium chlorides (BAC) in NaCl-containing aqueous media and further validated using additional testing systems of pure and mixed surfactants. This developed corrosion inhibition prediction model provides a potential method to evaluate the effectiveness of various surfactants in metal corrosion inhibition under various conditions of aqueous media.

Keywords: Inhibition efficiency; mixed surfactants; cmc; integrated model and prediction

1. INTRODUCTION

As an important component of the economy, the oil and gas industry has received considerable attention because oil mining and transportation have become increasingly expensive due in part to equipment damage caused by corrosive media, such as media containing dissolved H_2S, Cl^-, and CO_2 [1-5]. As a specific oil and gas industry example, pipeline made of carbon steel is easily corroded in environments that contain water and carbon dioxide (CO_2) [4-6]. The annual direct cost of corrosion in United State has been estimated to be around $276 billion or 3.1% of the gross domestic product

(GDP). About 3.7% out of the total cost comes from the oil and gas industry [3, 8], which is much of due to the CO_2 corrosion of carbon steel.

CO_2 is usually present in produced "sweet" fluids in the form of a dissolved gas and carbonic acid [9, 10]. Corrosion occurs when steel comes in contact with carbonic acid, which leads to the failure of pipelines, accidents, and economic losses. CO_2 corrosion is affected by many factors based on studies over the past several decades [8,11]: the change in temperature can lead to a change in CO_2 corrosion [12-14] and chemical composition of corrosion product [9,15]; the increase in CO_2 partial pressure [13,16] and fluid flow rate [17-19] accelerate CO_2 corrosion; the increase in pH [9,12,16], solution salt concentration such as Cl^- [20], and Cr [21] content in the steel matrix can decrease the uniform corrosion rate. In addition, O_2 can accelerate CO_2 corrosion by acting as a catalyst [22] and H_2S can increase corrosion through its synergistic action with CO_2 [23].

These concerns have led to great interest in industry and academia to control CO_2-related corrosion of pipeline in various oilfields around the world. A widely used corrosion control method is to use organic inhibitors, many of which are surfactants with hydrophilic and hydrophobic molecular sections [24-26]. It is usually assumed that the corrosion inhibition is equal to the effective surface coverage of surfactant inhibitor on steel [27-29]. However, there are many other factors that influence the performance and inhibition efficiency of surfactant, such as surfactant molecule structure, mixed composition of surfactant mixture, the material the surfactant is applied to and surface conditions (roughness, defects, etc.), and the environment in which the surfactants are used (fluid flow, salt concentration, temperature, pressure, etc.), etc. Extensive research work has been performed in the understanding of these processes but many challenges remain [30-36].

At present, the modeling of corrosion inhibition performance of surfactant inhibitors is limited to traditional methods, including Langmuir, Temkin, and Frumkin etc. [29, 37-41]. First-principles modeling, which is actually semi-empirical modeling based on best-fit of experimental data such as quantitative structure activity relation (QSAR) [42-46], combined QSAR and mechanistic approaches is also established. Multiphysics modeling, based on various processes that affect inhibition efficiency, such as fluid flow, pH, speciation, and partitioning [34, 47-49], is also available. However, each of these techniques is at different stages of maturity and has potential limitations.

Table 1. Experimental condition for different testing systems

Testing system	Mixed molar ratio α_i (C12Cl/C14Cl/C16Cl)	Salt (M)	Measured cmc (μM)	T (°C)	pH	Rotation speed (RPM)
I	0.70/0.25/0.05	0.171	144	40	4	300
II	0.33/0.33/0.33	0.599	16.5	40	5	100

In the present study, a model for the prediction of corrosion inhibition efficiency using surfactants (both pure and mixture) in aqueous media is introduced based on previous work [27-

29,37,50,51]. This model is based on the utilization of Langmuir adsorption (LA) sub-model with a critical micelle concentration (cmc) prediction sub-model. The developed model is referred to as a modified Langmuir adsorption (MLA). The predictive MLA model are developed and validated using electrochemical data collected from corrosion inhibition testing systems listed in Table 1, which include Testing System I and Testing System II. The predicted results from MLA agree well with experimental results. The MLA model is further extended to literature reported testing systems and demonstrates its wide applicability.

2. EXPERIMENTAL PROCEDURES AND MATERIALS

The surfactants used in this study are homologous cationic surfactants BAC, including benzyl dimethyl dodecyl ammonium chloride (C12Cl), benzyl dimethyl tetradecyl ammonium chloride (C14Cl), and benzyl dimethyl hexadecyl ammonium chloride (C16Cl) with assay values higher than 99%. The chemical structure of various surfactant molecules discussed in the present work is given in Fig. 1.

A piece of X65 steel was used as the working electrode in electrochemical measurements with a surface area of 0.196 cm^2. The composition (wt %) is C 0.06%, Mn 1.33%, P 0.007%, S 0.005%, Si 0.30%, Cu 0.30%, Ni 0.10%, V 0.022%, Cb 0.046%, Al 0.019%, Cr 0.05%, Mo 0.03%, Ti 0.017%, Ca 0.0033%, and Fe (balance).

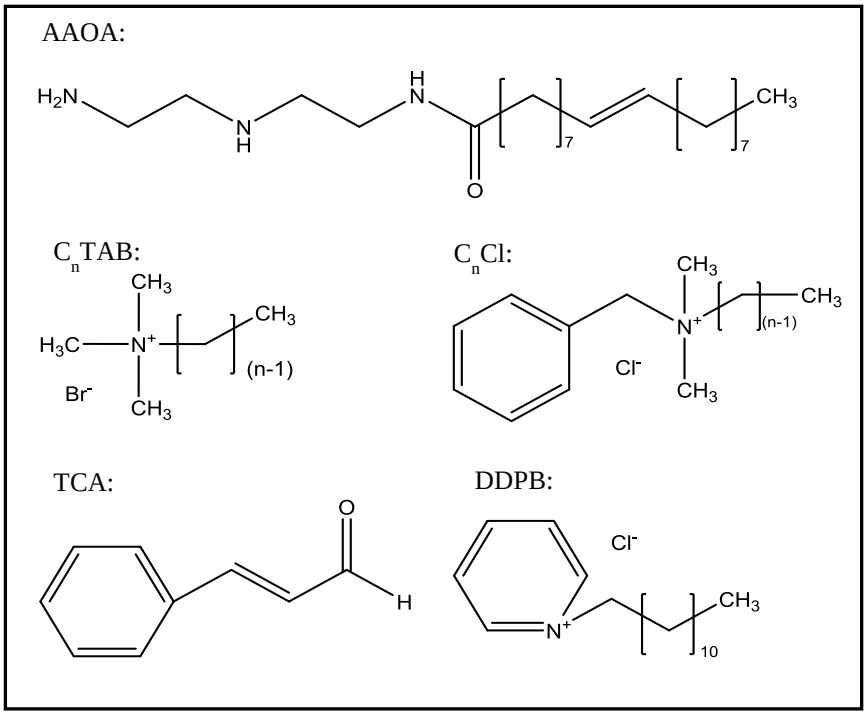

Figure 1. Chemical structure of various surfactant molecules discussed in the present work. n represents hydrocarbon chain length. AAOA: N-[2-[(2-aminoethyl) amino] ethyl]-9-octadecenamide; C_nCl: n-benzalkonium chloride; C_nTAB (or C_nTABr): n-alkyl trimethyl ammonium bromide; TCA: trans-cinnamaldehyde; DDPB: dodecylpyridinium bromide.

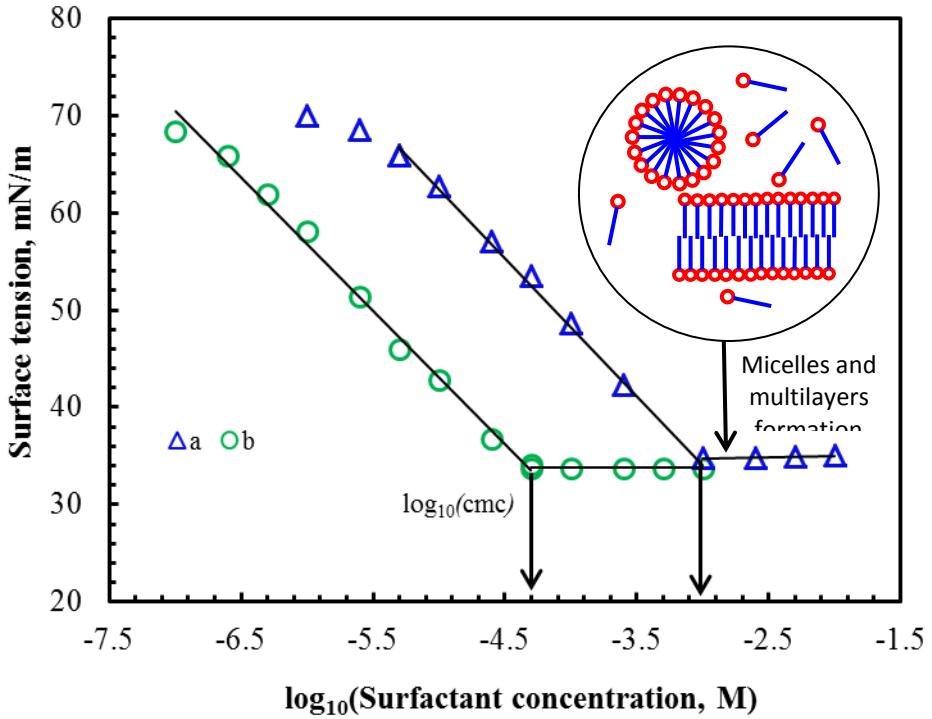

Figure 2. Plots of surface tension versus concentration of surfactants: (a) C12Cl in 0.171 M NaCl-containing aqueous solution at 40°C; (b) mixed C12Cl, C14Cl, & C16Cl at molar ratio of 0.15/0.70/0.15 in 0.171 M NaCl-containing aqueous solution at 40°C. The cmc value is indicated by the arrow.

The surface of the X65 electrode was polished using SiC paper in the sequence of 400-600-800-1200 grit, followed by polishing using polishing cloth with a particle size of ~ 5 μm supplied by Buehler. A platinum ring electrode and a single junction saturated calomel electrode (SCE) were employed as counter and reference electrodes, respectively. Test solutions contained 0.171 or 0.599 M NaCl and were purged with Ar (>99.999%) for 2 hours (hrs) to remove oxygen followed by a purge of CO_2 (>99.999%) for 2 hrs to ensure CO_2 saturation prior to measurements. A flow of CO_2 was maintained during the experiments to keep a positive pressure inside the cell to avoid air ingress. The pH was adjusted to 4 - 5 for different mixtures by the addition of 1.0 M $NaHCO_3$ or diluted HCl. The surfactants were added at the beginning of each measurement. The test solutions were then kept at open circuit potential, E_{corr}, for 2 hours for equilibration. Test conditions for different mixed surfactant systems are listed in Table 1. Testing System I is used as the primary example for the results discussion and inhibition efficiency prediction model derivation.

Polarization resistance R_p was measured using the linear polarization resistance (LPR) method by polarizing the working electrode +/- 0.010 V (SCE) vs. E_{corr} with a sweep rate of 0.1 mV/s. The slope of the tangent at the origin provided the value of R_p. Potentiodynamic scans were performed with a sweep rate of 1mV/s from -0.9 V (SCE) to -0.35 V (SCE). Each test was repeated at least three times as an independent measurement.

The test samples for surface tension measurements were prepared by sequential dilution of concentrated aqueous solutions of surfactants using double deionized water. The stock solution was

prepared at a total surfactant concentration of 25 mM for electrochemical measurements using deionized water. The surface tension of test solutions was measured within a precision of 0.1 mN/m by the platinum ring setup, equipped with an isothermal vessel holder. All the measurements were performed at a constant temperature of 40 ± 0.2°C, which has been shown to be higher than the Krafft point of the surfactants and their mixtures in aqueous media containing various concentrations of NaCl. The constant temperature was maintained through a water circulation bath. The platinum ring was rinsed with water and heated to an orange color using a Bunsen burner between tests to ensure the complete removal of contaminants. Triplicate measurements were used to confirm reproducibility. All values of reported surface tension were determined through the aforementioned procedures. Example of surface tension measurement of solution containing surfactants is shown in Fig. 2, in which the cmc of surfactants can be determined.

3. RESULTS AND DISCUSSION

3.1 Stability of Open Circuit Potential

Considering the stability of open circuit potential E_{corr} is important to electrochemical measurements, the X65 steel electrode was immersed in testing solution and kept at OCP for equilibration before measurement. Examples of the dependence of E_{corr} of X65 steel electrode on time in 0.171 M NaCl-containing aqueous media at 40°C are given in Fig. 3. The E_{corr} stabilized at around -0.725 V (SCE) without surfactant. It is reported that a positive shift of E_{corr} is usually observed upon the addition of surfactant into brine-containing aqueous media which is also saturated with CO_2 [52]. It can be seen from Fig. 3 that E_{corr} is stabilized between -0.640 V (SCE) and -0.740 V (SCE) after the introduction of surfactants over a wide concentration range, which includes the surface aggregation concentration (sac) and the cmc which is around 144 μM based on surface tension measurement. E_{corr} only increases slightly at surfactant concentrations above the cmc. The difference in E_{corr} in the absence and presence of surfactant indicates that the steel surface was covered and protected by the inhibitor adsorption. According to Riggs Jr. [53], it is feasible to classify one inhibitor as anodic type or cathodic type if the presence of inhibitor shifts E_{corr} at least +85 mV or -85 mV, respectively, relative to E_{corr} in the absence of inhibitor. However, the positive shift of E_{corr} of Testing System I at the highest concentration of 360 μM is only around 85 mV which suggests that both the dissolution of iron at the anode and the hydrogen evolution at the cathode were affected.

3.2 Potentiodynamic Scans and Linear Polarization Resistance Measurements

The potentiodynamic scan curves of Testing System I with various surfactant concentrations are presented in Fig. 4. Tafel slopes were estimated from these curves to calculate corrosion current density using the Tafel slope method. Note that there is no sensible linearity in the anodic branch in potentiodynamic scans as seen in Fig. 4 at the concentration above 72 μM, and thus the associated anodic Tafel slopes were derived from the cathodic branch [28,29]. The corrosion inhibition efficiency, *IE* (*%*), was calculated using Equation (1) [28,29,37,50].

$$IE\ (\%) = 100 \times \frac{i_{corr,o} - i_{corr}}{i_{corr,o}} \quad (1)$$

where $i_{corr,o}$ and i_{corr} are the corrosion current density without and with corrosion inhibitors/surfactants in solution respectively.

The polarization resistance was measured from LPR measurements and was then used to evaluate corrosion inhibition efficiency using Equation (2) with the Tafel slopes estimated from the curve of potentiodynamic scans.

$$IE(\%) = 100 \times \frac{R_p - R_{p,o}}{R_p} \quad (2)$$

where $R_{p,o}$ and R_p are polarization resistance in the absence and presence of corrosion inhibitors/surfactants respectively.

The results of Tafel slopes, polarization resistance, corrosion rate, and inhibition efficiency are summarized in Table 2 for the Testing System I. The corrosion inhibition efficiency results from potentiodynamic scans and linear polarization resistance (LPR) measurements are very close. Inhibition efficiency increases rapidly to around 90% with the increase in surfactant concentration up to 72 μM. Further increase in concentration does not effectively enhance inhibition efficiency even when the concentration is much higher than the cmc, C_{cmc}. The concentration of 72 μM is interpreted as the value of sac, C_{sac}, at which a complete monolayer usually forms at the electrode-solution interface, and above which, bilayers, multilayers, and semi-micelles usually form at the electrode-solution interface [28,29,37,50]. It has been reported that corrosion inhibition is directly associated to the electrode surface coverage [28,29,37,50], and therefore, the monolayer is much more effective in metal corrosion inhibition and the adsorption of bilayers/multilayers and semi-micelles on metal surface do not contribute much to additional corrosion inhibition.

Table 2. Tafel slopes, corrosion current density, polarization resistance, and *IE* (%) for X65 in the absence and presence of Testing System I with different surfactant concentrations

Total Concentration (μM)	β_a (mV dec^{-1})	$-\beta_c$ (mV dec^{-1})	i_{corr} (μA cm^{-2})	*IE* (%)[a]	R_p (ohm·cm^2)	*IE* (%)[b]
0	61.5	255	202	0	104	0
9	65.7	248	118	42	188	44
18	67.1	243	89	56	249	58
36	68.3	235	53	74	436	76
54	63.2	245	34	83	643	83
72	64.8	239	26	87	845	88
100	61.7[c]	238	13	94	1591	93
140	67.9[d]	237	9	96	2550	96
180	61.6[e]	245	7	97	2958	96
360	63.2[f]	233	5	98	4282	98

[a]*IE* (%) calculated from potentiodynamic scans; [b]*IE* (%) calculated from LPR; [c & d]derived from the cathodic branch and β_c due to lack of sensible linearity in the anodic branch in potentiodynamic scans as seen in Fig. 4. [28,29].

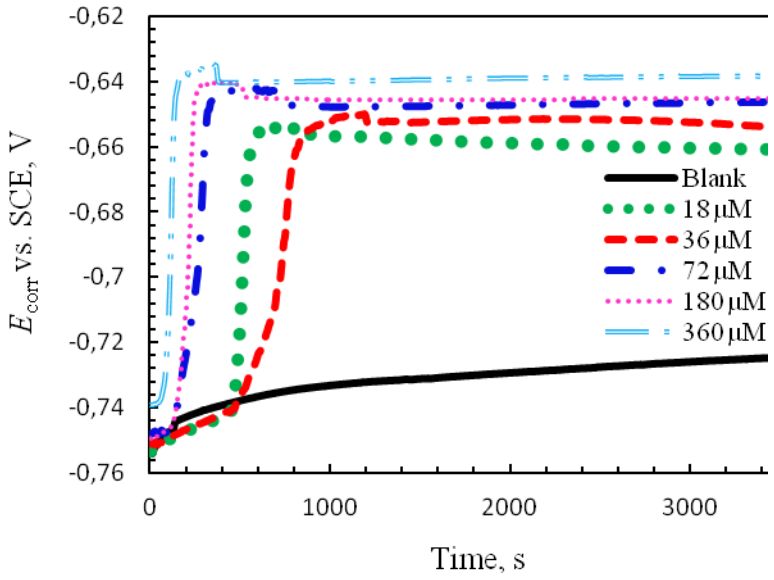

Figure 3. Variation of open circuit potential E_{corr} with time of X65 electrode immersed in aqueous conditions of Testing System I: CO_2-saturated 0.171 M NaCl-containing media with pH=4 in the absence of surfactant and presence of mixed C12Cl/CC14Cl/C16Cl=0.70/0.25/0.05 at different concentrations.

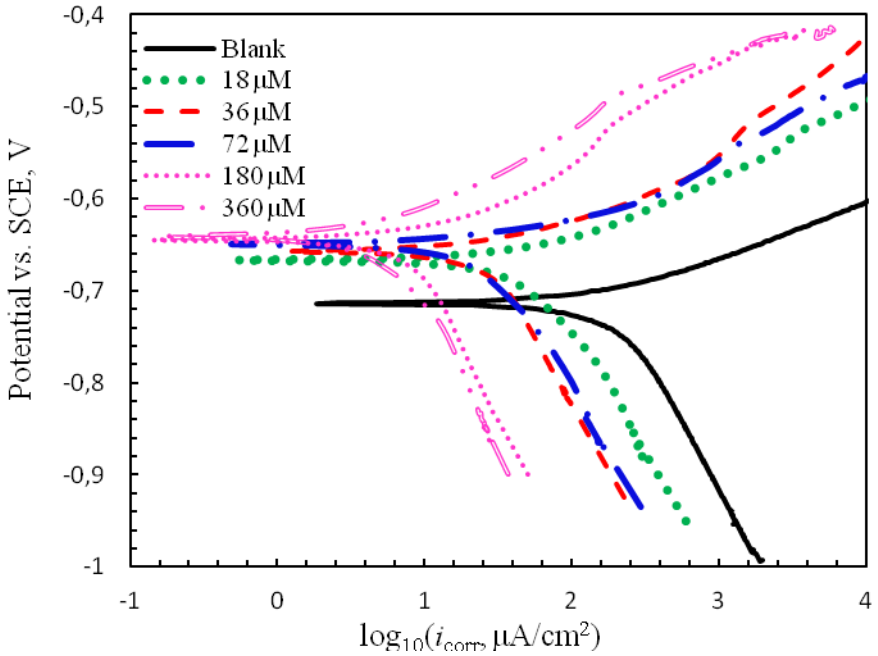

Figure 4. Potentiodynamic scan curves of X65 steel electrode exposed in Testing System I with and without surfactants.

3.3 Traditional Modeling Background

Corrosion inhibition assumes that the steel electrode corrodes uniformly and that the corrosion current density in the absence of surfactants, $i_{corr,o}$, is usually represented by the total number of surface

sites available for corrosion, whereas the corrosion current density in the presence of low concentration of inhibitor (usually lower than the cmc or sac), i_{corr}, is represented by the number of uncovered surface sites remaining after limited surfactant adsorption [28,29,37,50]. Thus, the surface coverage θ is assumed to be the fraction of surface sites covered by surfactant adsorption relative to the total surface sites and can be given by the expression:

$$\theta = \frac{i_{corr,o} - i_{corr}}{i_{corr,o}} = 1 - \frac{i_{corr}}{i_{corr,o}} \quad (3)$$

The adsorption of surfactants at the surface/interface is usually modeled by a traditional adsorption model. One of the widely accepted models is the Langmuir adsorption isotherm [28,29,37], in which the surface coverage is represented by:

$$\theta = \frac{K_{ad} C}{1 + K_{ad} C} \quad (4)$$

or

$$\frac{1}{\theta} = \frac{1}{K_{ad} C} + 1 \quad (5)$$

K_{ad} is given by

$$K_{ad} = \frac{1}{55.5} \exp\left(-\frac{\Delta G^{o}_{ad}}{RT}\right) \quad (6)$$

where K_{ad} is equilibrium adsorption constant, C is the concentration of total surfactants in the bulk solution, the value 55.5 is the molar concentration of water in solution in unit moles per liter (M), ΔG^{o}_{ad} is the standard free energy of the adsorption process, R is gas constant, and T is absolute temperature. Note that for pure surfactant, C and C_{cmc} are total concentration of pure surfactant i, C_i, in solution and its corresponding cmc, $C_{cmc,i}$, respectively; for mixed surfactants, C and C_{cmc} are total concentration of mixed surfactants, C_{mix}, in solution and their corresponding mixed cmc, $C_{cmc,mix}$, respectively.

A plot of ($1/\theta$) vs. $1/C$ (for $C < C_{cmc}$) using Equation (5) based on LPR of Testing System I yields an intercept which gives an equilibrium constant K_{ad} of a value of 8.13×10^4 M^{-1}, as shown in Fig. 5. C_{cmc} represents the value of cmc. ΔG^{o}_{ad} is calculated and the value is -39.8 kJ·mol^{-1}. The negative value demonstrates that the adsorption of surfactant on the steel surface is a spontaneous process and shows a strong interaction between surfactant molecules and steel surface [54]. Generally, if adsorption free energy is more positive than -20 kJ·mol^{-1}, the interaction between surfactant and metal is classified as physisorption due to electrostatic interaction. When the adsorption free energy is more negative than -40 kJ·mol^{-1}, the adsorption involves charge sharing or transfer between surfactant molecules and metal surface to form coordination bonds, which is also classified as chemisorption [55]. Based on the calculated value of adsorption free energy, -39.8 kJ·mol^{-1}, the adsorption mechanism of the discussed mixture can be classified as the combination of chemisorption and physisorption. Specifically, the adsorption mechanism of surfactant on steel electrode surface is often interpreted as follows: the unpaired or π electrons of the surfactant molecule and the vacant d orbitals of iron share electrons (chemisorption); the charged surfactant and electrode surface interact through electrostatic force (physisorption). However, physisorption can sometimes be energetically favorable and significant whereas chemisorption may sometimes have relatively weak binding energy due to various factors that influence adsorption [56,57].

3.4 Modified Langmuir Adsorption Model

A combination of Equations (3) and (4) and rearrangement lead to a useful equation that correlates the corrosion current density to surfactant concentration [29,37]:

$$\frac{1}{i_{corr}} = \frac{1}{i_{corr,o}} + \frac{K_{ad}C}{i_{corr,o}} \quad (7)$$

There should be a linear relationship between the inverse of corrosion current density ($1/i_{corr}$) and bulk surfactant concentration C when $C \leq C_{sac}$. The surfactant adsorption and corrosion inhibition at this level is particularly effective with increasing concentration due to plenty of active surface sites available to be covered by surfactants. Above the sac, an abrupt transition should occur in the slope, because the electrode surface is covered by a complete monolayer. Increasing concentration of the surfactant above the sac should lead to the formation of bilayers/multilayers and micelles (above cmc), which slightly contribute to surface coverage and corrosion inhibition.

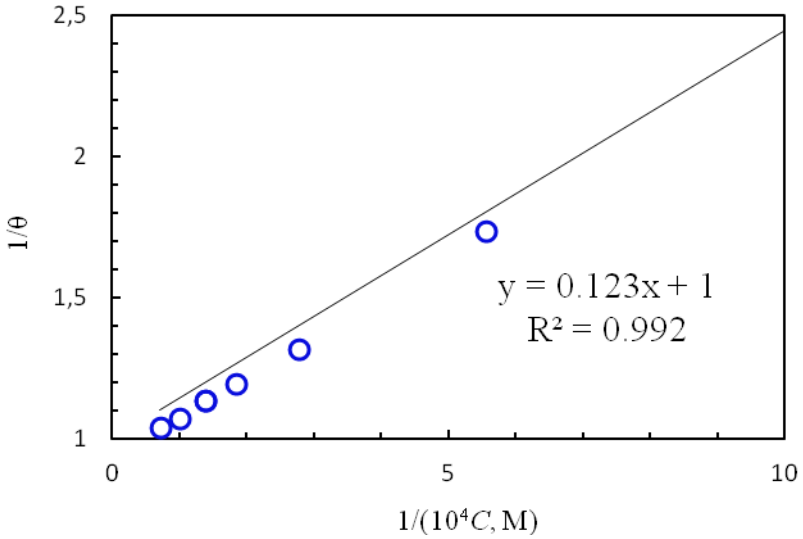

Figure 5. Plot of ($1/\theta$) vs. $1/C$ using Equation (5) based on LPR measurements

Thus, the sac is an important scaling factor in the determination of the effect of surfactant concentration on adsorption and corrosion inhibition. However, because the cmc is easier to measure than the sac in the present research and due to the availability of a developed prediction model for cmc, the concentration in Equation (7) is normalized by dividing by C_{cmc}, rather than by C_{sac}, and rearranged to give:

$$\frac{1}{i_{corr}} = \frac{1}{i_{corr,o}} + \frac{K}{i_{corr,o}}\frac{C}{C_{cmc}} \quad (8)$$

where K is equal to the adsorption constant K_{ad} multiplied by C_{cmc} of surfactant. Further rearrangement leads to a general form which can be used to evaluate corrosion of a variety of surfactants under a variety of test conditions:

$$\frac{1}{1-\theta} = \frac{i_{corr,o}}{i_{corr}} = 1 + K\frac{C}{C_{cmc}} \quad (9)$$

Note homologous surfactants tend to achieve similar levels of surface coverage at similar ratios of surfactant concentration to surfactant cmc, so the value of *K* does not vary a lot for homologous surfactants. Note that *C* could increase above the sac or the cmc, but the fitting is generally not as good as the fitting for *C* below the sac.

The measured cmc for the surfactant mixture in Testing System I, 0.70/0.25/0.05 in 0.171M NaCl aqueous media at 40°C, is 144 μM. A plot of $\frac{i_{corr,o}}{i_{corr}}$ versus $\frac{C}{C_{cmc}}$ yields a slope of constant *K*=13.74, and an intercept of 1 which is in the absence of inhibitor, as shown in Fig. 6. There is one abrupt transition around the concentration of the sac, which indicates that when the inhibitor concentration is below the sac, inhibition efficiency increases rapidly with the increases in concentration; above the sac, the increase in concentration does not contribute much to further inhibition efficiency increase.

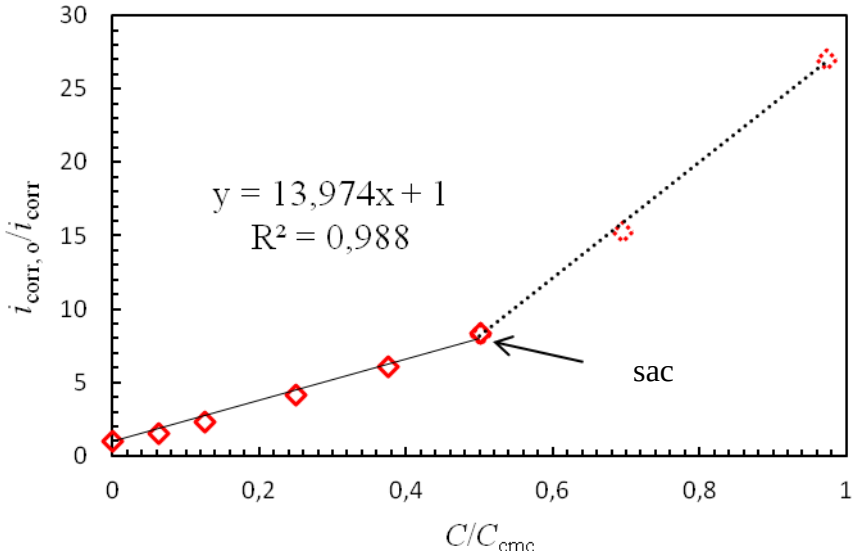

Figure 6. Plot of $\frac{i_{corr,o}}{i_{corr}}$ versus $(\frac{C}{C_{cmc}})$ of X65 steel exposed in CO2-saturated 0.171 M NaCl aqueous solution containing various concentrations of mixed surfactants C12Cl, C14Cl, & C16Cl at molar ratio of 0.70/0.25/0.05 at 40°C.

3.5 The cmc Prediction Sub-model

It is noticed from previous discussion that the cmc is required for the use of MLA model regarding corrosion inhibiton prediction and therefore, one cmc prediction sub-model is introduced in this section.

Despite extensive progress in theoretical and experimental work has been made in the study of aggregation properties of ionic surfactants the effect of added salt and specific ion (dissociated from surfactants and salt) is still a challenge [37,51,58]. The ion and salt usually shift cmc, aggregation number of micelle, sphere-to-rod transition, and counterion binding coefficient [51,58,59]. The micelle shape, micelle composition (for mixed surfactants), and micelle distribution are also affected

[51,58,59]. In the present work an improved cmc prediction sub-model based on existing molecular thermodynamic theory [58] has been introduced for various pure and mixed surfactants. Activities of monomeric surfactant and counterion, which are evaluated from Setchenov equation [60] and Pitzer's method [61] or Davies [62] equation respectively, are incorporated. The specific headgroup-counterion pair is introduced to model counterion specificity. The effect of coion is reflected from salt-dependent factors, including Setchenov coefficient, dielectric decrement of salt, and the correlation between surface tension and salt concentration of aqueous solution. The developed cmc sub-model has been applied to various surfactants in aqueous solution containing various salt concentrations for validation [37,50,51]. More details about the sub-model derivation and validation can be found in supplementary information and existing references [37,50,51].

Assuming the monomeric surfactant m_i (i represents surfactant 1, 2, or 3...) is completely dissociated in aqueous solution containing counterion m_j (j=1, 2, or 3…) but in the micelle form the surfactant is associated to some extent with counterions, therefore, the surfactant micellization is described by the following process [37,50,51].

$$n\sum_i \alpha_i m_i^{z_i} + n\sum_j \delta_j m_j^{z_j} \leftrightarrow M_{n\alpha_i\delta_j}^{n\left(\sum_i \alpha_i z_i + \sum_j \delta_j z_j\right)} \quad (10)$$

where α_i is the composition of surfactant i in the micelle, $M_{n\alpha i\delta j}$, which has an aggregation number n, micelle composition α_i, and a counterion binding coefficient δ_j. For micelles of pure surfactant, $\alpha_i = 1$; for mixed micelles, $0 < \alpha_i < 1$. z_i and z_j are the valences of ionic surfactant i in dissociated form and counterion j. For nonionic surfactant i, $z_i = 0$ and $\delta_j = 0$.

By the consideration of activity coefficient, the chemical potential of micelle $M_{n\alpha i\delta j}$, monomeric surfactant i, and counterion j in solution can be written, respectively, as

$$\mu_{n\alpha_i\delta_j} = \mu^\circ_{n\alpha_i\delta_j} + kT\ln(a_{n\alpha_i\delta_j}) = \mu^\circ_{n\alpha_i\delta_j} + kT\ln(\gamma_{n\alpha_i\delta_j} X_{n\alpha_i\delta_j}) \quad (11)$$

$$\mu_{mi} = \mu^\circ_{mi} + kT\ln(a_{mi}) = \mu^\circ_{mi} + kT\ln(\gamma_{mi} X_{mi}) \quad (12)$$

$$\mu_{mj} = \mu^\circ_{mi} + kT\ln(a_{mj}) = \mu^\circ_{mj} + kT\ln(\gamma_{mj} X_{mj}) \quad (13)$$

where $\mu^\circ_{n\alpha_i\delta_j}$, μ°_{mi} and μ°_{mi} are the standard chemical potentials of micelle, monomeric surfactant, and counterion in solution, respectively. The standard state of water is defined as pure liquid while the standard state of all other species is defined for an infinitely dilute solution. $a_{n\alpha i\delta j}$, a_{mi}, and a_{mj} are the corresponding activities. $\gamma_{n\alpha i\delta j}$, γ_{mi}, and γ_{mj} are the corresponding activity coefficients. Micelle is treated as one separated phase from aqueous solution and thus $\gamma_{n\alpha i\delta j} = 1$. $X_{n\alpha i\delta j}$, X_{mi}, and X_{mj} are mole fractions of micelle, monomeric surfactant, and counterion in bulk solution.

The cmc is assumed to be equal to monomer concentration and the monomer molar fraction X_m is calculated by [37,50,51].

$$X_{cmc} = \exp^{\left(\frac{1}{kT}\Delta\mu^\circ_m\right)} \quad (14)$$

The micellization free energy $\Delta\mu^\circ_m$ is estimated from a few contributing terms as described below:

$$\Delta\mu^\circ_m = \Delta\mu^\circ_{trt} + \Delta\mu^\circ_{int} + \Delta\mu^\circ_{pack} + \Delta\mu^\circ_{st} + \Delta\mu^\circ_{ent} + \Delta\mu^\circ_{elec} + \Delta\mu^\circ_{act} \quad (15)$$

where $\Delta\mu^\circ_{trt}$, $\Delta\mu^\circ_{int}$, $\Delta\mu^\circ_{pack}$, $\Delta\mu^\circ_{st}$, $\Delta\mu^\circ_{ent}$, and $\Delta\mu^\circ_{elec}$ are the free energy contributions from hydrocarbon transfer from water into micelle, formation of micellar core-water interface, hydrocarbon tail packing in the micelle, surfactant headgroup steric interaction, headgroup-counterion mixing, and electrostatic interaction, respectively [37,50,51]. $\Delta\mu^\circ_{act}$ comes from the activity contribution [37,50,51].

Free energy micellization as a function of variables, including micelle shape, micelle composition α_i, micellar core minor radius, and counterion binding coefficient δ_j (j represents ion), at given solution conditions is minimized using home-designed MATLAB code. The minimized micellization free energy is then used for the evaluation of cmc, aggregation number, counterion binding coefficient, and sphere-to-rod transition. Details of free energy calculation is reported elsewhere [37,50,51].

The model is applied to pure alkyltrimethylammonium surfactant C16TAB in solution with added salt (NaBr, NaCl, or KCl) to evaluate chain length effects, counterion effects, and coion effects on aggregation properties as shown in Fig. 7. The cmc (Fig. 7(a)) and sphere-to-rod transition threshold (Fig. 7(b)) decreases as chain length increases whereas n_w (Fig. 7(b)) increases as chain length increases. The predicted cmc for all surfactants in Fig. 7 match very well with the experiment except that slight deviation appears for C12TAB with added NaBr above 1 M. Excellent agreement is observed between predicted and experimental n_w. The transition threshold of salt concentration is well predicted as indicated by the change of n_w. For C16TAB with KBr for example, the predicted threshold is 0.08 M and the experimental threshold is 0.1 M [63].

The model is further applied to ternary mixed homologous benzalkonium chloride surfactants CnCl. C12Cl and C16Cl are equal-molar mixed with varying molar fractions of C14Cl at different NaCl concentrations. The data and its comparison with the model are presented in Fig. 8, which demonstrate the wide applicability of the present cmc model.

3.6 Corrosion Inhibition Prediction

The corrosion inhibition efficiency can be predicted using the equation below based on the developed MLA model

$$IE\ (\%) = 100\theta = \left(1 - \frac{1}{K\frac{C}{C_{cmc}}}\right) \times 100 \qquad (16)$$

Fig. 9 presents the comparison of predicted inhibition efficiency and experimental inhibition efficiency for different testing systems using both MLA and Langmuir adsorption (LA). The K value for mixed BAC is obtained by fitting the MLA model to the experimental data of Testing System I. The model is validated using the data obtained from Testing System II. The sac of Testing System II is estimated to be 9 μM, at which the inhibition efficiency is around 90% and above which inhibition efficiency is slightly increased as the concentration continues to increase. The predicted corrosion inhibition efficiency of Testing System II using regular LA model is also presented in which significant deviation between prediction and experimental data is observed due to the lack of solution condition adjustment using cmc. This is attributed to the different solution conditions for Testing System I and Testing System II in which the aggregation properties, such as cmc and micelle composition, of mixed BAC are different and thus K_{ad} values differ. In MLA, K_{ad} is replaced by incorporating the cmc to obtain universal constant K for homologous BAC. The corrosion inhibition efficiency prediction model is also extended to other surfactant testing systems and works very well, such as AAOA-1018 steel system [5], C16TAB-copper system [27], and TCA-DDPB-J55steel system [69], as shown in Fig. 9.

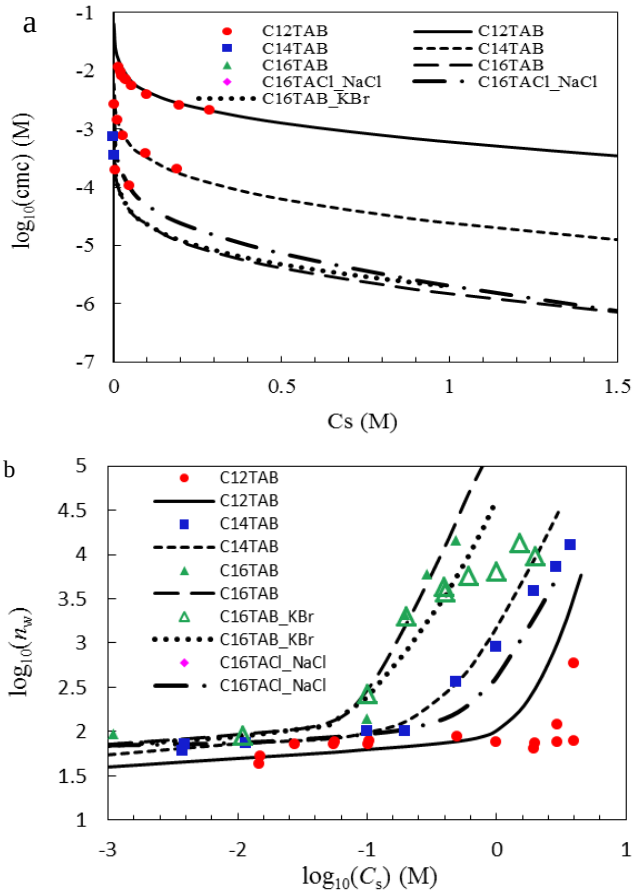

Figure 7. (a) cmc and (b) weight-based aggregation number n_w of alkyltrimethylammonium bromide/chloride C_nTAX ($X=B^-/Br^-$ and Cl^-) vs. salt concentration. The salt type is specified as it is in the legend; if not specified the salt is NaBr. Solid and dashed lines represent model prediction; symbols represent experimental data cited from references [63,64-68]. Model inputs based on experimental conditions: 35°C, and total solution concentration of surfactant set at 10 mM for C14TAB and C16TAB/Cl and set at 30 mM for C12TAB.

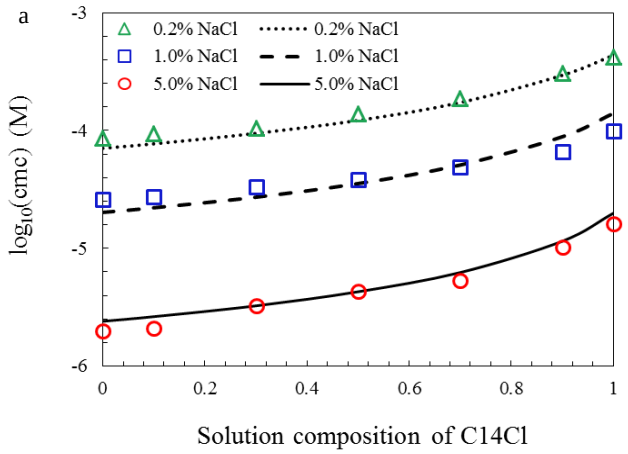

Figure 8. cmc vs. solution molar composition of C14Cl in ternary mixed C12Cl, C14Cl, & C16Cl in aqueous solution, in which C12Cl & C16Cl are equal-molar mixed. Solid and dashed lines represent model prediction; symbols represent experimental data [51].

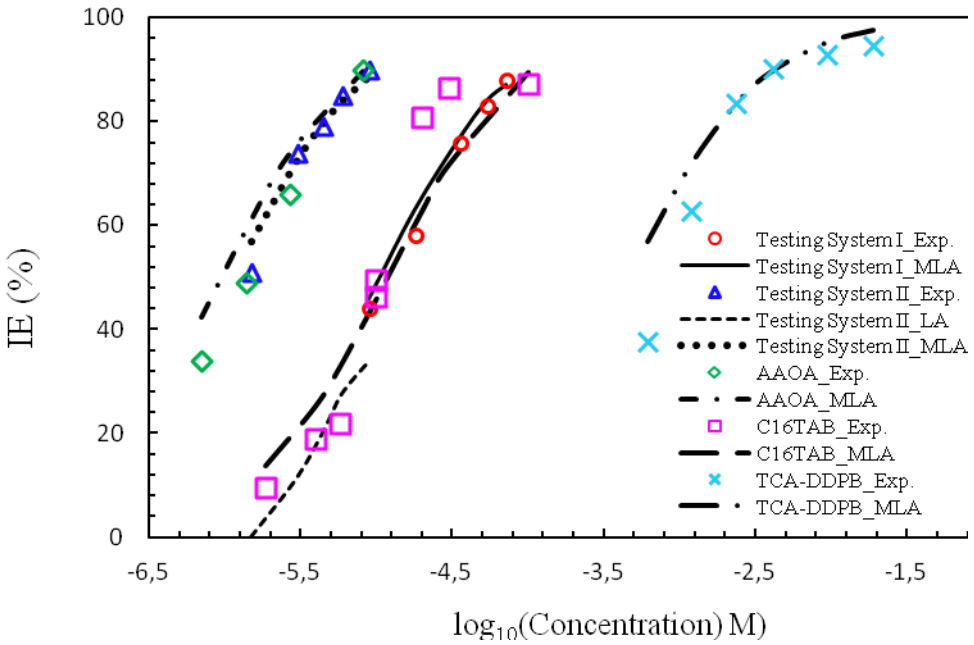

Figure 9. Comparison between experimental inhibition efficiency and predicted inhibition efficiency for Testing Systems I and II listed in Table 1 and for reported testing systems using surfactant AAOA [5], surfactant C16TAB [24], and mixed surfactants TCA and DDPB based on MLA and LA. *K′* are 15.73 for AAOA in 0.856 M NaCl aqueous solution at 25°C, 2.52 for C16TAB in 0.03 M $Fe(NO_3)_3$ aqueous solution at 32°C, 20.26 for mixed TCA and DDPB in 10% HCl aqueous solution at 30 °C. The values of the cmc for AAOA, C16TAB, and mixed TCA and DDPB in the discussed solution environment are 15 μM, 9.8 μM, and 9.5 mM, respectively.

4. CONCLUSIONS

Corrosion inhibition efficiency rapidly increases as the surfactant concentration increases to the sac, indicating the formation of a relatively complete surfactant monolayer around the sac that effectively protects the metallic electrode from corrosion. A new cmc prediction sub-model for various pure and mixed surfactants is developed over a wide concentration range of salt. The improved corrosion inhibition efficiency prediction model MLA which incorporates LA and the cmc prediction is an effective method that can be used for corrosion inhibition prediction of various ternary mixtures of homologous BAC surfactants at various salt concentrations. In addition, this MLA model provides a potential method to evaluate cmc and corrosion inhibition efficiency of pure surfactant, and binary-, ternary-, or multiple-component mixtures of surfactants of interest in aqueous media containing salt. In addition, a modified Quantitative Structure Activity Relation (MQSAR) model which is equivalent to MLA can be found elsewhere for potential readers [37].

ACKNOWLEDGEMENTS
The presented research is supported by a grant from BP. CHPC at the University of Utah is acknowledged for providing computational resources.

References

1. B. Tribollet, J. Kittel, A. Meroufel, F. Ropital, F. Grosjean, and E. M. M. Sutter, *Electrochim. Acta*, 124 (2014) 46.
2. Y. Zhu and M. L. Free, *Int. J. Corros. Scale Inhib*., 4 (2015) 311.
3. P. Bai, H. Zhao, S. Zheng, and C. Chen, Corros. Sci., 93 (2015) 109.
4. Y. Zhou and Y. Zuo, *Electrochim. Acta*, 154 (2015) 157.
5. D.A. López, S.N. Simison, and S.R. de Sánchez, *Electrochim. Acta*, 48 (2003) 845.
6. K.S. George and S. Nešić, *Corrosion*, 63 (2007) 178.
7. B.R. Linter, G.T. Burstein, *Corros. Sci*., 41 (1999) 117.
8. N. G. Thompson, Y. Mark, and D. Daniel, *Corros. Rev*., 25 (2007) 247.
9. C. de Waard and D.E. Milliams, *Corrosion*, 31 (1975) 177.
10. G.I. Ogundele and W.E. White, *Corrosion*, 43 (1987) 665.
11. A. Ikeda, S. UedaM, Mukai, *NACE International Corrosion Conference*, New Orleans (1984).
12. K. Videm and A. Dugstad, *Mater. Perform*., 4 (1989) 46.
13. B. Mishra, S. Al-Hassan, D.L. Olson, and M.M. Salama, *Corrosion*, 53 (1997) 852.
14. M.B. Kermani and A. Morshed, *Corrosion*, 59 (2003) 659.
15. M.H. Ezuber, *Mater. Des*., 30 (2009) 3420.
16. S. Nešić, J. Postlethwaite, and S. Olsen, *Corrosion*, 52 (1996) 280.
17. S. Nešić and L. Lunde, *Corrosion*, 50 (1994) 717.
18. C. de Waard, U. Lotz, and A. Dugstad, *NACE International Corrosion Conference*, Houston (1995).
19. J.C. Cardoso Filho and M.E. Orazem, *NACE International Corrosion Conference*, Houston (2001).
20. Q.Y. Liu, L.J. Maoa, and S.W. Zhou, *Corros. Sci*., 84 (2014) 165.
21. C.F. Chen, M.X. Lu, D.B. Sun, Z.H. Zhang, and W. Chang, *Corrosion*, 61 (2005) 594.
22. K. Videm and A. M. Koren, *Corrosion*, 49 (1993) 746.
23. B. Brown, S.R. Parkala, and S. Nesic, *NACE International Corrosion Conference* (2003).
24. R. Fuchs-Godec, *Electrochim. Acta*, 54 (2009) 2171.
25. D. Gelman, D. Starosvetsky, and Y. Ein-Eli, *Corros. Sci*., 82 (2014) 271.
26. B. Kronberg, *Curr. Opin. Colloid Interface Sci*., 2 (1997) 456.
27. M. L. Free, *Corros. Sci.*, 46 (2004) 3101.
28. Y. Zhu, M. L. Free, and G. Yi, The Effects of Surfactant Concentration, Adsorption, Aggregation, and Solution Conditions on Steel Corrosion Inhibition and Associated Modeling in Aqueous Media *Corros. Sci*., (2015). in press.
29. Y. Zhu, M. L. Free, and G. Yi, *Corros. Sci*., 98 (2015) 417.
30. S. Endo and K. Goss, *Environ. Sci. Technol*., 48 (2014) 2776.
31. M. A. Cowell, T. C. G. Kibbey, J. B. Zimmerman, and K. F. Hayes, *Environ. Sci. Technol*., 34 (2000) 1583.
32. J. Iyer and D. Blankschtein, *J. Phys. Chem. B*, 118 (2014) 2377.
33. V. Srinivasan and D. Blankschtein, *Langmuir*, 19 (2003): pp. 9946-9961.
34. C. D. Taylor, A. Chandra, J. Vera, and N. Sridhar, *J. Electrochem. Soc*., 162 (2015) 369.
35. A. Kokalj, S. Peljhan, M. Finsgar, and I Milosev, *J. Am. Chem. Soc*., 132 (2010) 16657.
36. A. Kokalj, *Corros. Sci*., 68 (2013) 195.
37. Y. Zhu, M. L. Free, *J. Electrochem. Soc*., 162 (2015) C582.
38. Y. Zhu, M. L. Free, *J. Electrochem. Soc*., 162 (2015) C702.
39. R. Fuchs-Godec, *Colloid. Sur. A: Physicochem. Eng. Aspects*, 280 (2006) 130.
40. M. Farsak and H. Keles, M. Keles, *Corros. Sci*., 98 (2015) 223.
41. M. P. Kern and D. Landolt, *Corros. Sci*., 47 (2005) 485.
42. I. B. Obot, D. D. Macdonald, and Z. M. Gasem, *Corros. Sci*., (2015).
43. G. Gece, *Corros. Sci*., 50 (2008) 2981.
44. Sonu, A. K. Tiwari, and S. K. Saha, *Ind. Eng. Chem. Res*., 52 (2013) 5895.

45. G.Gece, *Corros. Sci*., 53 (2011) 3873.
46. H. Zhao, X. Zhang, L. Ji, H. Hu, and Q. Li, *Corros. Sci*., 83 (2014) 261.
47. D. A. Winkler, M. Breedon, A. E. Hughes, F. R. Burden, A. S. Barnard, T. G. Harvey, and I. Cole, *Green Chem*., 16 (2014) 3349.
48. L. Li, X. Zhang, S. Gong, H. Zhao, Y. Bai, Q. Li, and L. Ji, *Corros. Sci*., (2015).
49. S. K. Mondal, and S. R. Taylor, *J. Electrochem. Soc*., 161 (2014) C476.
50. Y. Zhu and M. L. Free, *ECS Trans*., 66 (2015) 53.
51. Y. Zhu and M. L. Free, *Ind. Eng. Chem. Res.*, 54 (2015) 9052.
52. M. Knag, K. Bilkova, E. Gulbrandsen, P. Carlsen, and J. Sjoblom, *Corros. Sci*., 48 (2006) 2592.
53. O. L. Riggs Jr., *Corrosion Inhibitors*, 2nd ed., Houston (1973).
54. M. Christov and A. Popova, *Corros. Sci*., 46 (2004) 1613.
55. P. C. Okafor and Y. Zheng, *Corros. Sci*., 51 (2009) 850.
56. X. Shi, R. Zhang, C. Minot, K. Hermann, M. A. Van Hove, W. Wang, and N. Lin, *J. Phys. Chem. Lett.*, 1 (2010) 2974.
57. J. N. Israelachvili, *Intermolecular and Surface Forces*, 3rd ed., Academic Press, San Diego (2011).
58. L. Moreira and A. Firoozabadi, *Langmuir*, 26 (2010) 15177.
59. N. Vlachy, B. Jagoda-Cwiklik, R. Vácha, D. Touraud, P. Jungwirth, and W. Kunz, *Adv. Colloid Interface Sci.*, 146 (2009) 42.
60. R. P. Schwarzenbach, P. M. Gschwend, and D. M. Imboden, *Environmental Organic Chemistry*, 2nd Ed., John Wiley, New York (2001).
61. J. F. Zemaitis, D. M. Clark, M. Rafal, and N. C. Scrivner, *Handbook of Aqueous Electrolyte Thermodynamics*, AlChE, New York (1986).
62. J. N. Butler, *Ionic Equilibrium: Solubility and pH Calculations*, John Wiley, New York, 1998.
63. Z. Weican, L. Ganzuo, M. Jianhai, S. Qiang, Z. Liqiang, L. Haojun, and W. Chi, *Chin. Sci. Bull.*, 45 (2000) 1854.
64. S. Ozeki and S. Ikeda, *Colloid Polym. Sci*., 262 (1984) 409.
65. T. Imae, R. Kamiya, and S. Ikeda, *J. Colloid Interface Sci*., 108 (1985) 215.
66. T. Imae and S. Ikeda, *J. Phys. Chem*., 90 (1986) 5216.
67. H. Nomura, S. Koda, T. Matsuoka, T. Hiyama, R. Shibata, and S. Kato, *J. Colloid Interface Sci*., 230 (2000) 22.
68. A. Khatory, F. Lequeux, F. Kern, and S.J. Candau, *Langmuir*, 9 (1993) 1456.
69. F. B. Growcock and W. W. Frenier, *J. Electrochem. Soc*., 135(1988) 817.